Inorganic Chemistry

Article

pubs.acs.org/IC

Conventional and Stuffed Bergman-Type Phases in the Na−Au−T (T = Ga, Ge, Sn) Systems: Syntheses, Structures, Coloring of Cluster Centers, and Fermi Sphere−Brillouin Zone Interactions

Qisheng Lin, Volodymyr Smetana, Gordon J. Miller,* and John D. Corbett*

Ames Laboratory, U.S. Department of Energy, and Department of Chemistry, Iowa State University, Ames, Iowa 50011, United States

Supporting Information

ABSTRACT: Bergman-type phases in the Na−Au−T (T = Ga, Ge, and Sn) systems were synthesized by solid-state means and structurally characterized by single-crystal X-ray diffraction studies. Two structurally related (1/1) Bergman phases were found in the Na−Au−Ga system: (a) a conventional Bergman-type (CB) structure, $Na_{26}Au_xGa_{54-x}$, which features empty innermost icosahedra, as refined with x = 18.1 (3), $Im\bar{3}$, a = 14.512(2) Å, and Z = 2; (b) a stuffed Bergman-type (SB) structure, $Na_{26}Au_yGa_{55-y}$, which contains Ga-centered innermost icosahedra, as refined with y = 36.0 (1), $Im\bar{3}$, a = 14.597(2) Å, and Z = 2. Although these two subtypes have considerable phase widths along with respective tie lines at Na ≈ 32.5 and 32.1 atom %, they do not merge into a continuous solid solution. Rather, a quasicrystalline phase close to the Au-poor CB phase and an orthorhombic derivative near the Au-rich SB phase lie between them. In contrast, only Au-rich SB phases exist in the Ge and Sn systems, in which the innermost icosahedra are centered by Au rather than Ge or Sn. These were refined for $Na_{26}Au_{40.93(5)}Ge_{14.07(5)}$ ($Im\bar{3}$, a = 14.581(2) Å, and Z = 2) and $Na_{26}Au_{39.83(6)}Sn_{15.17(6)}$ ($Im\bar{3}$, a = 15.009(2) Å, and Z = 2), respectively. Occupations of the centers of Bergman clusters are rare. Such centering and coloring correlate with the sizes of the neighboring icosahedra, the size ratios between electropositive and electronegative components, and the values of the average valence electron count per atom (e/a). Theoretical calculations revealed that all of these phases are Hume−Rothery phases, with evident pseudogaps in the density of states curves that arise from the interactions between Fermi surface and Brillouin zone boundaries corresponding to a strong diffraction intensity.

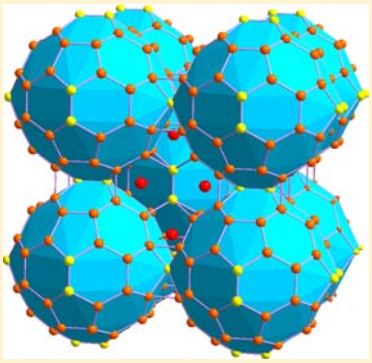

INTRODUCTION

Recent exploratory syntheses of Au-rich polar intermetallics have established a substantial role for Au in stabilizing new phases that display many fascinating structural motifs originating from the strong bonding between Au and many of the post-transition metals and metalloids.[1,2] In contrast to Au-poor phases, in which Au atoms often participate in the formation of polyanionic clusters or networks, pure Au fragments are commonly seen in Au-rich polar intermetallics, such as aggregates of Au_4 tetrahedra in Rb_2Au_3Tl,[3] one-dimensional rods of hexagonal Au stars in $Ca_{14}Au_{46}Sn_5$,[4] two-dimensional undulating Au layers in $Ca_4Au_{10}In_3$,[5] and three-dimensional diamond-like extended frameworks, such as in Ba_2Au_8Sn.[6] Although these pure Au fragments are aggregated and bound, not isolated, or naked, they are reminiscent of small isolated, charged, or neutral Au clusters in the gas phase or solutions, e.g., Au_n^- (n = 1−4),[7] Au_7,[8] Au_{11},[9] Au_{15-19},[10] Au_{20},[11,12] and so on, and of colloidal or nanocrystalline Au with beautiful shapes.[13,14] The availability of various Au fragments in intermetallics may open new insight to bridging the science from atoms to clusters and to bulk materials. It might also be worthwhile to carry out explorations of Au-rich polar intermetallics for catalytic properties.

From the viewpoint of valence electron counts, Au-rich polar intermetallics generally have small e/a values (valence electron counts per atom) because the $5d^{10}$ states are customarily not counted and thus electronically approach the so-called Hume-Rothery phases.[15−17] The last term refers to those phases with peculiar structure types such as γ-brass, e.g., Cu_5Zn_8,[17] in which Fermi spheres (nearly) touch the surface boundaries of similarly sized Brillouin zones and, thus, open energy gaps for certain regions of reciprocal space. This effect creates pseudogaps in the density of states (DOS) curves. Therefore, the study of Au-rich phases may aid in the generation of new ideas for materials that are electronically positioned between polar intermetallics and the Hume-Rothery phases.

In past years, our explorations of ternary Au systems uncovered several novel Au-rich phases within the K−Au−Sn,[18] K−Au−Ga,[19] and Ca−Au−T (T = Ga,[20,21] In,[22] Ge,[23] Sn[4,24]) systems. The K and Ca series produce strikingly different products in the Au-rich (or low e/a) regions. Generally, YCd_6-type quasicrystals and their corresponding approximants are found in the Ca−Au−T (T = Ga,[20] In,[22] Ge,[23] Sn[24]) systems, but none of these exists in the K−Au−Sn and K−Au−Ga systems. The reason may be 2-fold: (i) the metallic radius of K is much larger than that of Ca (2.349 vs 1.97 Å for CN = 12)[25] so that K requires more neighboring

Received: April 27, 2012
Published: August 3, 2012

   dx.doi.org/10.1021/ic300866q | Inorg. Chem. 2012, 51, 8882−8889

Table 1. Loaded Compositions, Products, and Lattice Parameters (22 °C) Refined from Powder and/or Single-Crystal Data for Na−Au−Ga Bergman Phases

no.	Na/Au/Ga	products and estimated yields[a]	powder[b]	single cryst	cryst no.
1	50/16.6/33.3	70% CB + 20% $Na_{30}Au_5Ga_{55}$ + 10% Na	14.5095(8)	14.512(2)	**1**
2	40/20/40	70% CB + 30% $Na_{30}Au_5Ga_{55}$	14.4926(8)	14.492(2)	**S1**
3	32.5/22.5/45	80% CB + 20% $Na_{30}Au_5Ga_{55}$	14.4779(8)		
4	32.5/26.3/41.3	>95% CB	14.4771(8)		
5	32.5/30.0/37.5	65% QC + 35% CB			
6	32.5/33.8/33.8	55% QC + 45% CB			
7	32.5/37.5/30.0	>95% $Na_{32}Au_{38}Ga_{30}$			
8	32.5/45.0/22.5	50% SB + 40% $Na_{32}Au_{38}Ga_{30}$ + 10% Na_2Au_3Ga	14.5628(8)		
9	40/40/20	>95% SB	14.6094(8)	14.593(2)	**S2**
10	20/55/25	30% SB + 40 $NaAu_3Ga_2$ + 30% $NaAu_2$		14.597(2)	**2**

[a]CB denotes a *conventional* Bergman type with an empty Wyckoff 2a (0 0 0) site; SB denotes a *stuffed* Bergman type with the 2a site occupied by Ga, and QC denotes an icosahedral quasicrystal. [b]Lattice parameters were refined from the five strong diffraction peaks between 35° and 45°, if distinguishable from peaks of other phases.

Table 2. Crystal and Structural Refinement Data for the CB Type $Na_{26}Au_{18.1(3)}Ga_{35.9(3)}$ (1) and the SB Types $Na_{26}Au_{36.0(1)}Ga_{19.0(1)}$ (2), $Na_{26}Au_{40.93(5)}Ge_{14.07(5)}$ (3), and $Na_{26}Au_{39.83(6)}Sn_{15.17(6)}$ (4)

	1	2	3	4
formula	$Na_{26}Au_{18.1(3)}Ga_{36.9(3)}$	$Na_{26}Au_{36.0(1)}Ga_{19.0(1)}$	$Na_{26}Au_{40.93(5)}Ge_{14.07(5)}$	$Na_{26}Au_{39.83(6)}Sn_{15.17(6)}$
e/a	1.90	1.47	1.52	1.56
fw	6665.8	9008.8	9680.9	10243.4
space group, Z	$Im\bar{3}$, 2	$Im\bar{3}$, 2	$Im\bar{3}$, 2	$Im\bar{3}$, 2
unit cell a (Å)	14.512(2)	14.597(2)	14.581(2)	15.009(7)
Vol. (Å^3), ρ_{cal} (g/cm^3)	3056.2(6), 7.244	3110.2(6), 9.620	3099.9(7), 10.372	3381(3), 10.061
reflns collcd/R_{int}	13597/0.0968	13769/0.0980	13506/0.1137	14757/0.0944
data/restraints/param	726/0/42	726/0/43	715/0/41	776/0/41
GOF	1.155	1.068	1.110	1.084
R1/wR2 [$I > 2\sigma(I)$]	0.0369/0.0578	0.0289/0.0589	0.0329/0.0585	0.0324/0.0650
R1/wR2 (all data)	0.0555/0.0623	0.0381/0.0626	0.0504/0.0619	0.0382/0.0673
peak/hole (e/Å^3)	2.320/−2.241	2.225/−3.197	2.753/−3.389	2.313/−4.730

atoms; (ii) the energy difference between the 3d and 4s orbitals of K is larger than that of Ca, for which the 3d orbitals are energetically close to its highest-occupied 4s orbitals. This smaller 3d−4s energy difference in Ca enhances possible d−sp orbital mixings, which help the formation of pseudogaps in Ca-containing quasicrystals and approximants.[17,20,22,24] On the other hand, the valence electron counts required for the formation of YCd_6-type approximants and quasicrystals (both Hume-Rothery phases) fall short in the analogous K-containing systems.

Recently, we have focused on the exploration of Na−Au−Ga systems for novel robust structures and potentially interesting electronic properties, and two new polar intermetallic phases, $Na_{0.56}Au_2Ga_2$ and $Na_{13}Au_{41.2}Ga_{30.3}$, with tunnel-like structural motifs were discovered.[26] As we continued investigations on the Na−Au−T (T = Ga, Ge, Sn) systems, Bergman phases emerged in all of these systems. Generally, in Bergman structures, the Wyckoff 2a sites that center the inner icosahedral clusters are empty. In this work, we have found two subtypes of Bergman-type structures with slightly differentiated motifs: the conventional type with an empty 2a site and the stuffed type with an occupied 2a site. Although Bergman and Pauling originally reported partial occupancy at the 2a site in $Mg_{32}(Al,Zn)_{49}$,[27] no such occupation has been confirmed.[28,29] It should also be noted that Ge- and Sn-containing Bergman phases were previously reported as $Na_{26}Au_{40}Ge_{15}$ and $Na_{30}Au_{39}Sn_{12}$.[30] However, the chemically unreasonable Na/Au admixtures in the latter system also encouraged us to reinvestigate their structures.

EXPERIMENTAL SECTION

Synthesis. Starting materials included Na ingots (99.95%, Alfa Aesar), with surfaces manually cleaned with a surgical blade, as-received Au particles (99.999%, Ames Laboratory), Ga ingots, Ge pieces, and Sn shot (all 99.999%, Alfa Aesar). Reaction mixtures, ca. 400 mg total for each, were weighed in a N_2-filled glovebox (H_2O < 0.1 ppmv), loaded into precleaned Ta tubes ($\phi \sim 0.9$ mm) that were sealed by arc welding under Ar, and then enclosed in evacuated SiO_2 jackets (<10^{-5} Torr). The Ga-containing samples were heated at 750 or 800 °C for 6−10 h, cooled to 350 °C at a rate of 5−10 °C/h, then annealed there for 2−6 days, and quenched into water. All Ge- and Sn-containing samples were obtained through a similar reaction profile: heated at 700 °C for 6 h, cooled to 400 °C at a rate of 2 °C/h, annealed there for 6 days, and quenched into water.

Table 1 lists the more important reactions carried out in the Na−Au−Ga system, together with products and refined lattice parameters for the desired Bergman phases. Two types of Bergman phases were found: (1) a conventional Bergman (CB) type with empty innermost icosahedra within the Bergman clusters; (2) a stuffed Bergman (SB) type, in which the cluster center is fully occupied by Ga atoms. An icosahedral quasicrystal and an orthorhombic derivative of the Bergman phase were also found lying between these two Bergman subtypes.[31]

For the Ge- and Sn-containing Bergman phases, samples with nominal compositions of "$Na_{26}Au_{40}Ge_{15}$" and "$Na_{30}Au_{39}Sn_{12}$"[30] were first tried. The former yielded the desired pure phase that was later refined as $Na_{26}Au_{40.93(5)}Ge_{14.07(5)}$, but the latter under the same conditions produced a mixture of mostly a Bergman-type phase

dx.doi.org/10.1021/ic300866q | Inorg. Chem. 2012, 51, 8882−8889

Table 3. Atomic Coordinates and Isotropic Equivalent Displacement Parameters for the CB Type $Na_{26}Au_{18.1(3)}Ga_{35.9(3)}$ (1) and the SB Types $Na_{26}Au_{36.0(1)}Ga_{19.0(1)}$ (2), $Na_{26}Au_{40.93(5)}Ge_{14.07(5)}$ (3), and $Na_{26}Au_{39.83(6)}Sn_{15.17(6)}$ (4)

atom[a]	Wyckoff	symm	x	y	z	U_{eq} (Å^2)	occ. ≠ 100%
$Na_{26}Au_{18.1(3)}Ga_{35.9(3)}$ (1)							
M1	48h	1	0.15348(3)	0.40435(3)	0.19041(3)	0.0217(2)	58.1/41.9(7)
M2	24g	*m*..	0	0.15271(6)	0.09375(6)	0.0120(3)	22.5/77.5(5)
Ga3	24g	*m*..	0	0.30824(9)	0.18546(9)	0.0153(5)	
M4	12e	*mm*2..	0.0950(1)	0	$^1/_2$	0.0457(7)	24.2/75.8(7)
Na1	24g	*m*..	0	0.1157(3)	0.3064(3)	0.024(1)	
Na2	16f	0.3.	0.1889(2)	*x*	*x*	0.020(1)	
Na3	12e	*mm*2..	0	$^1/_2$	0.3040(5)	0.025(2)	
$Na_{26}Au_{36.0(1)}Ga_{19.0(1)}$ (2)							
M1	48h	1	0.15127(3)	0.40378(3)	0.18676(3)	0.0172(2)	88.2/11.8(4)
Au2	24g	*m*..	0	0.16382(3)	0.09936(3)	0.0105(2)	
Ga3	24g	*m*..	0	0.3107(1)	0.1906(1)	0.0126(4)	
M4	12e	*mm*2..	0.0904(1)	0	$^1/_2$	0.0364(6)	46.9/53.1(7)
Ga5	2a	*m*-3.	0	0	0	0.0082(9)	
Na1	24g	*m*..	0	0.1109(5)	0.3099(5)	0.017(2)	
Na2	16f	0.3.	0.1899(3)	*x*	*x*	0.015(2)	
Na3	12e	*mm*2..	0	$^1/_2$	0.3027(5)	0.015(2)	
$Na_{26}Au_{40.93(5)}Ge_{14.07(5)}$ (3)							
Au1	48h	1	0.1458(1)	0.4032(1)	0.1888 (1)	0.012(1)	
Au2	24g	*m*..	0	0.1643(1)	0.1028(1)	0.010(1)	
Ge3	24g	*m*..	0	0.3069(1)	0.1988(1)	0.010(1)	
M4	12e	*mm*2..	0.0862(1)	0	1/2	0.032(1)	65.5/34.5(8)
Au5	2a	*m*-3.	0	0	0	0.007(1)	
Na1	24g	*m*..	0	0.1157(4)	0.3055(4)	0.018(1)	
Na2	16f	0.3.	0.1888(3)	*x*	*x*	0.015(1)	
Na3	12e	*mm*2..	0	$^1/_2$	0.3047(7)	0.011(2)	
$Na_{26}Au_{39.83(6)}Sn_{15.17(6)}$ (4)							
Au1	48h	1	0.1525(1)	0.4049(1)	0.1868(1)	0.011(1)	
Au2	24g	*m*..	0	0.1596(10	0.0975(1)	0.008(1)	
Sn3	24g	*m*..	0	0.3096(1)	0.1890(1)	0.009(1)	
M4	12e	*mm*2..	0.0904(1)	0	$^1/_2$	0.024(1)	47/53(1)
Au5	2a	*m*-3.	0	0	0	0.004(1)	
Na1	24g	*m*..	0	0.1179(4)	0.3046(4)	0.017(1)	
Na2	16f	0.3.	0.1902(3)	*x*	*x*	0.015(2)	
Na3	12e	*mm*2..	0	$^1/_2$	0.3027(6)	0.012(2)	

[a]M = Au/T (T = Ga, Ge, or Sn).

($Na_{26}Au_{38.54(4)}Sn_{13.45(4)}$), a trace amount of $NaAu_2$, and an unidentified phase. So, the refined composition, $Na_{26}Au_{38.5}Sn_{13.5}$, was reacted under the same conditions, and a pure phase product of $Na_{26}Au_{39.83(6)}Sn_{15.17(6)}$ was obtained according to powder X-ray diffraction. Later, parallel reactions with different Au/Ge and Au/Sn proportions, i.e., $Na_{26}Au_xSn_{54-x}$ (x = 32, 34, and 36, with e/a = 1.83, 1.68, and 1.60) and $Na_{26}Au_yGe_{55-y}$ (y = 37 and 43, with e/a = 1.67 and 1.44), were reacted with the aim of checking the availability of CB phases, icosahedral quasicrystals, and the phase widths of SB phases. However, all listed reactions always produced a majority Bergman-type phase, together with orthorhombic NaAuGe or cubic $NaAu_2$.

All of the Bergman-type phases show metallic luster and appear to be inert to air at room temperature according to powder X-ray diffraction patterns. However, the surfaces of the Ga samples subjected to scanning electron micropscopy−energy-dispersive X-ray analyses were found to have been oxidized on contact with water during the polishing process.

X-ray Diffraction. Phase analyses were performed on the basis of powder diffraction data collected at room temperature using a STOE Stadi P powder diffractometer or Huber G670 camera, both equipped with an image plate and Cu Kα_1 radiation (λ = 1.540598 Å). Single crystals were mounted on a Bruker APEX CCD single-crystal diffractometer equipped with graphite-monochromatized Mo Kα (λ = 0.71069 Å) radiation. Room temperature intensity data were collected in an ω-scan method over 2 θ = ∼7−57° and with exposures of 10 s/frame. The reflections in all data sets were consistent with body-centered-cubic (bcc) symmetry. Data integration, Lorentz polarization, and other corrections (e.g., instrumental factors, polarization effects, decay effects) were accomplished by the *SAINT* subprogram included in the *SMART* software package.[32] Empirical absorption corrections were performed with the aid of the subprogram *SADABS*.

A total of seven structures were refined: four for Ga-containing, one for Ge-containing, and two for Sn-containing phases. The crystallographic data and structure refinements for a CB structure of $Na_{26}Au_{18.1(3)}Ga_{35.9(1)}$ (1) and three SB structures of $Na_{26}Au_{36.0(1)}Ga_{19.0(1)}$ (2), $Na_{26}Au_{40.93(5)}Ge_{14.07(5)}$ (3), and $Na_{26}Au_{39.83(6)}Sn_{15.17(6)}$ (4) are summarized in Table 2, and the refined positional parameters are given in Table 3, as standardized using *STRUCTURE TIDY*.[33] Panels a and b in the Supporting Information, Figure S1, show the good agreement between the experimental and simulated powder patterns of both $Na_{26}Au_{40.93(5)}Ge_{14.07(5)}$ and $Na_{26}Au_{39.83(6)}Sn_{15.17(6)}$. The crystallographic data for a CB structure of $Na_{26}Au_{19.5(4)}Ga_{34.5(4)}$ (**S1**), a SB structure of $Na_{26}Au_{35.2(1)}Ga_{19.8(1)}$ (**S2**), and a vacancy-ordered SB structure of $Na_{26}Au_{38.54\ (4)}Sn_{13.45(4)}$ (**S3**) are listed in Table S1 in the Supporting Information. Detailed crystallographic data for all seven crystals are available in the CIF outputs (Supporting Information).

dx.doi.org/10.1021/ic300866q | *Inorg. Chem.* 2012, 51, 8882−8889

Table 4. List of Some Bergman-Type Phases with Respective Lattice Parameters, Center-to-Vertex Distances of Innermost Shells (r), R_+/R_- Ratios, e/a Values, and Atomic Decorations at Different Sites

formula	a (Å)	r (Å)	R_+/R_-	e/a	2a	24g	24g	48f	12e	24g	16f	12e	ref
$Mg_{64}Al_{40.7}Zn_{55.3}$	14.271(1)	2.61	1.14	2.25		Zn/Al	Zn/Al	Zn/Al	Mg	Mg	Mg	Mg	29
$Li_{32.2}Mg_{19.8}Al_{81.2}Zn_{26.8}$	14.073(3)	2.52	1.11	2.31		Zn/Al	Zn/Al	Zn/Al	Al	Li/Mg	Li/Mg	Li	40
$Li_{52}Al_{86.2}Zn_{21.8}$	14.135(3)	2.54	1.10	2.21		Zn/Al	Zn/Al	Zn/Al	Al	Li	Li	Li	28
$Li_{52}Ni_{37}Si_{72}$	12.741	2.27	1.15	2.13		Ni/Si	Ni/Si	Ni/Si	Si	Li	Li	Li	30
$Li_{52}Cu_{57}Si_{51}$	12.933	2.33	1.17	1.96		Cu/Si	Cu/Si	Cu/Si	Cu/Si	Li	Li	Li	30
$Li_{13}Cu_6Ga_{21}$	13.568(2)	2.49	1.13	2.05		Ga	Cu	Ga	Ga	Li	Li	Li	41
$Li_{52}Cu_{19.3}Al_{88.7}$	13.9056(3)	2.52	1.11	2.11		Cu/Al	Cu/Al	Cu/Al	Al	Li	Li	Li	52
$Na_{16}Mg_{36}Al_{40}Zn_{68}$	14.2173(7)	2.52	1.23	2.15		Zn/Al	Zn/Al	Zn/Al	Al	Na/Mg	Na/Mg	Na/Mg	53
$Na_{13}Cd_{20}Pd_7$	15.992(2)	2.90	1.22	1.78		Cd/Pb	Cd	Cd/Pb	Cd/Pb	Na	Na	Na	48
$Na_{13}Cd_{18.9}Tl_{8.1}$	15.9121(5)	2.91	1.24	1.88		Cd/Tl	Cd	Cd/Tl	Cd/Tl	Na	Na	Na	39
$Na_{26}Au_{18.1}Ga_{35.9}$	14.512(2)	2.60	1.34	1.90		Au/Ga	Ga	Au/Ga	Au/Ga	Na	Na	Na	this work
$Na_{26}Au_{36.0}Ga_{19.0}$	14.597(2)	2.80	1.33	1.47	Ga	Au	Ga	Au/Ga	Au/Ga	Na	Na	Na	this work
$Na_{26}Au_{40.9}Ge_{14.1}$	14.581(2)	2.83	1.32	1.52	Au	Au	Ge	Au	Au/Ge	Na	Na	Na	this work
$Na_{26}Au_{39.8}Sn_{15.2}$	15.009(2)	2.81	1.27	1.56	Au	Au	Sn	Au	Au/Sn	Na	Na	Na	this work

Resistivity Measurements. Temperature-dependent resistivities were measured between 1.8 and 300 K using a standard, four-probe alternating-current (f = 16 Hz) technique in a Quantum Design PPMS instrument. Epotek H20E silver epoxy was used to attach Pt wires to the samples. The samples measured, $Na_{26}Au_{40.9}Ge_{14.1}$ (SB), $Na_{26}Au_{39.8}Sn_{15.2}$ (SB), and $Na_{26}Au_{18}Ga_{36}$ (CB), all yielded metal-like resistivities between 0.12 (Ga) and 0.26 (Ge) mΩ cm. The ρ_{10}/ρ_{300} values fell between 0.99 (Ga) and 0.90 (Sn) (Figure S2 in the Supporting Information).

Electronic Structure Calculations. Calculations for hypothetical "$Na_{26}Au_{24}Ga_{30}$" for CB and "$Na_{26}Au_{43}Sn_{12}$" for SB structures (described below) were performed by means of the self-consistent, tight-binding, linear-muffin-tin-orbital (LMTO) method in the local density and atomic sphere (ASA) approximations, using the Stuttgart code.[34−37] The automatically scaled ASA radii used in the "$Na_{26}Au_{24}Ga_{30}$" model were 3.37, 3.37, 3.30, 2.93, 2.91, 2.83, and 3.02 Å for Na1−Na3, Au1, Ga2−Ga4, respectively, whereas those for Na1−Na3, Au1−Au3, Sn4, and Au5 in "$Na_{26}Au_{43}Sn_{12}$" were 3.61, 3.52, 3.55, 3.10, 2.99, 3.00, 2.90, and 3.11 Å, respectively. Interstitial spheres were automatically inserted to achieve space filling for both models. The Ga model was inserted with only one empty sphere at the origin, with a radius of 2.88 Å, and the Sn model was inserted with two independent empty spheres, which are located beneath the T−T dimers in the fourth shell (see below), with radii of 1.26 and 1.06 Å). Reciprocal space integrations were carried out by means of the tetrahedron method. The basis sets were 3s/(3p) for Na, 5d/(5f)/6s/6p for Au, 4s/4p/(4d) for Ga, and 5s/5p/(5d) for Sn, with orbitals in parentheses down-folded.[38] Scalar relativistic effects were included in the calculations. The band structure was sampled for 24 × 24 × 24 k points in the irreducible wedge of the Brillouin zone.

RESULTS AND DISCUSSION

Phase Widths and Relationships with Binaries. According to literature data (cf. later Table 4), Bergman-type phases are generally solid solutions with appreciable phase widths. For example, the Zn atomic percentage in the parent $Mg_{32}(Al,Zn)_{49}$ Bergman phase can vary from 14.1% to 51.5%,[28,29] whereas the Tl atomic percentage in $Na_{13}(Cd,Tl)_{27}$ ranges over 16.2−22.3%.[39] A reason is that Bergman-type phases usually contain pairs of similarly sized atoms distributed among the electron-richer sites,[40] e.g., Al/Zn and Cd/Tl in foregoing phases, so that their mixing does not result in pronounced geometrical distortions. However, as a class of Hume-Rothery phases,[15−17] Bergman-type phases are also thought to be stabilized within certain ranges of valence electron counts, which may also limit the mixing among atoms with different valence electrons. $Li_{13}Cu_6Ga_{21}$[41] is probably the only line compound in this class.

According to our experimental results, two Bergman phases appear in the Na−Au−Ga ternary system along the tie lines with 32.5% and 32.1% atomic percentages of Na, as shown in Figure 1. A 1/1 CB phase, $Na_{26}Au_xGa_{54-x}$, lies in the Ga-richer

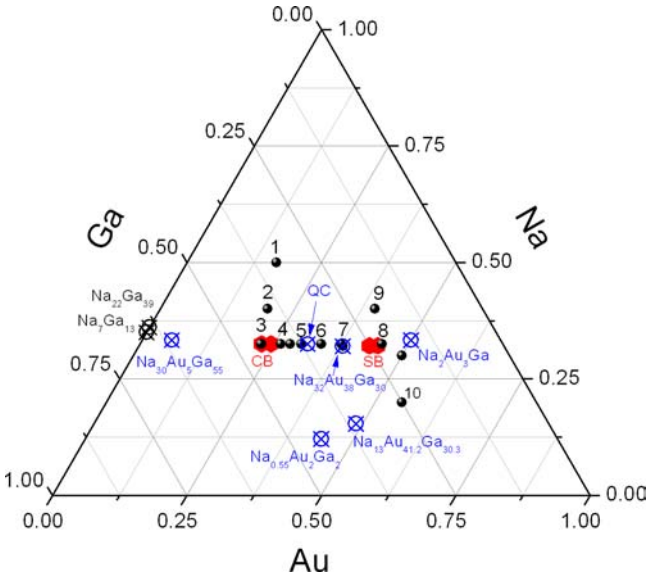

Figure 1. Phase distributions of the CB and SB phases (shaded in red) and others in the Na−Au−Ga system at ~350 °C. Blue circles with crosses denote related phases that have been structurally established, black spheres represent loaded compositions, and numbers refer to the reaction sequence listed in Table 1.

region, with $x \approx 18.1-19.5$, whereas SB phase $Na_{26}Au_yGa_{55-y}$ falls in the Au-richer region, with $y \approx 35.2-36.0$. Although wider phase boundaries are suggested for both CB and SB phases according to lattice parameters refined from powder data (Table 1), it is evident that these two phase regions do not merge. As a matter of fact, reactions with stoichiometries between these two regions yield mixtures of Bergman phases and an icosahedral quasicrystal phase.[31] A pure orthorhombic derivative of the Bergman phase, $Na_{32}Au_{38}Ga_{30}$ (*Cmcm*), was also found to the left of the SB phase region (Table 1). This is the first example in which two distinctive Bergman-type phases

dx.doi.org/10.1021/ic300866q | Inorg. Chem. 2012, 51, 8882−8889

exist in the same system, but a similar situation occurs for the Tsai-type approximants $M_3(Au,Ge)_{19}$ and $M_{3.25}(Au,Ge)_{18}$[23] in which a disordered $(Au,Ge)_4$ tetrahedron in the former is replaced by a single M atom (M = Ca, Yb).

In addition to the above Bergman and orthorhombic $Na_{32}Au_{38}Ga_{30}$ phases, three other compounds exist in this system that also feature Bergman-type clusters as building blocks, i.e., the binary Na_7Ga_{22} (*Pnma*[42] and $R\bar{3}m$[43]) and $Na_{22}Ga_{39}$ (*Pnma*[44]) and the ternary $Na_{30}Au_5Ga_{55}$ (*P6/mmm*)[31] phases; see also Figure 1. However, the Bergman-type clusters in all of these electron-richer phases are connected by bridging Ga atoms, in contrast to the condensation of Bergman clusters in CB and SB phases. Evidently, this phenomenon is related to the further formal oxidation incurred by the incorporation of more electron-poor Au in the latter systems.

In comparison, both Ge- and Sn-based Au-stuffed Bergman phases have small homogeneity ranges judging from their refined lattice parameters, which fall within 14.5905(8)−14.5980(8) Å for Ge-containing and 15.0011(8)−15.0462(8) Å for Sn-containing systems, with ranges of about 9.6σ and 39.9σ, respectively. Attempts have also been made to determine whether Ge- and Sn-containing systems also include the CB-type phases, which are supposed to have larger e/a values, i.e., in excess of ca. 1.78 (Table 4). However, the reaction targeting "$Na_{26}Au_{32}Ge_{22}$" (e/a = 1.83) produced a SB-type phase, orthorhombic NaAuGe,[45] and the cubic Laves phase $NaAu_2$.

Structures. Bergman-type phases are best described separately in terms of their short-range (the local geometries and decorations) and long-range (packing in three dimensions) order of Bergman clusters, as before.[27,29,46,47] All of the present structures feature bcc packing of Bergman-type clusters, with Na3 atoms as interstitials or fillers between these giant clusters, as shown in Figure 2. Each cluster consists of four endohedral shells: from the center out, an inner icosahedron, a dodecahedron, a larger icosahedron, and a buckminsterfullerene-like (M_{60}) cluster. The major differences among all Bergman phases concern the constitutions and decorations of these shells.

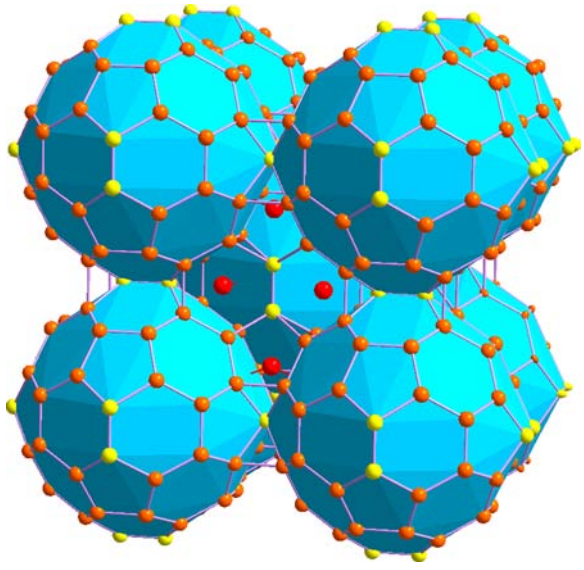

Figure 2. bcc packing of multiply endohedral clusters in the unit cell of Bergman-type phases. Note that the 24 red spheres denoting Na3 atoms in the present structures locate outside of the Bergman clusters; cf. Figure 3.

As shown in Figure 3, the innermost icosahedral shell is completely defined by 12 Au2 atoms in Au-richer crystals $Na_{26}Au_{36.0}Ga_{19.0}$ (**2**), $Na_{26}Au_{40.9}Ge_{14.1}$ (**3**), and $Na_{26}Au_{39.8}Sn_{15.2}$ (**4**) but by 12 mixed Au/Ga2 atoms in the Au-poor specimen $Na_{26}Au_{18.10}Ga_{35.90}$ (**1**; Table 3). Note that the size of this icosahedral shell is related to the occupation of the cluster center. For crystals **2**−**4**, the center-to-vertex radii of these Au_{12} as stuffed by Ga, Au, and Au are 2.7967(6), 2.8263(8), and 2.807(1) Å, respectively, whereas it is 2.601(1) Å in the Ga-richer but empty **1**. The inverse relationship between the Au_{12} radii and lattice parameters (Table 2) of the Ge- and Sn-containing phases (or the Ge or Sn sizes) seems unique.

The dodecahedral second shell (Figure 3) is defined by 12 Na1 and 8 Na2 atoms, with the latter on the body diagonals. This is the only shell containing electropositive atoms within Bergman-type clusters.[46] Each pentagonal face of this shell is capped by Au2 from the inner shell and by T atoms (T = Ga, Ge, or Sn) from the third shell.

The third shell is an icosahedron built solely of 12 T atoms (T = Ga, Ge, or Sn). This is an inflated icosahedral copy of the first shell, and no direct bonds exist between any two vertices within this shell. Rather, each vertex is connected to a vertex of the inner icosahedron by heteroatomic Au/Ga−Ga bonds (for **1**) and Au−T bonds (for **2**−**4**). Note that each of these 12 bonds is perpendicular to a pentagonal face of the dual dodecahedral shell and is collinear with one of the 12 pseudo-5-fold axes of the Bergman clusters. Likewise, the 12 atoms in the third-shell icosahedron also lie above the centers pentagonal faces in the fourth shell.

The buckminsterfullerene-like cage is the outmost shell of what is called a Bergman cluster. This shell is defined by atoms generated from the Wyckoff 12e and 48h positions. For crystals **1** and **2**, all 60 vertices are occupied by mixed Au/Ga atoms, i.e., Au/Ga1 and Au/Ga4. In comparison, the 48 vertices generated from the Wyckoff 48h sites are pure Au1 in crystals **3** and **4**, whereas the 12 vertices from Wyckoff 12e sites are occupied by Au/Ge4 or Au/Sn4 mixtures (Table 3). The mixed atoms at 12e sites form six pairs of dimers, each lying in the unit cell faces (Figure 3). It should be noted that these nominal dimer units always have the largest displacement parameters (Table 3), with the ellipsoids elongated orthogonal to the bond direction. This effect might be related to the large void beneath the dimers (into which empty spheres are inserted in the LMTO calculations); it also indicates a possible configurational or occupancy disorder, as observed in $Na_{26}Au_{38.54(4)}Sn_{13.45(4)}$ (**S3**; Table S1 in the Supporting Information).

Beyond the Bergman cluster, there remains another shell defined by 24 Na3 atoms (Figure 3). These Na3 atoms, together with Na2 atoms (not shown) that cap faces of the former's eight hexagonal faces (which are actually also the vertices of the second shell of neighboring clusters), define a triacontahedron. However, if this shell is considered as a repeating unit, two neighboring triacontahedra overlap along body-diagonal directions, a feature that requires a description in terms of interpenetrating clusters and shared atoms. Nevertheless, such condensed triacontahedra are still legitimate building units of quasicrystals and approximants.[2,46]

Differences from Literature Data for Ge- and Sn-Containing Phases. In general, our refinements for **3**, $Na_{26}Au_{40.93(5)}Ge_{14.07(5)}$, confirm the structural data of $Na_{26}Au_{40}Ge_{15}$ reported by Schuster and coworkers,[30] but the

dx.doi.org/10.1021/ic300866q | *Inorg. Chem.* 2012, 51, 8882−8889

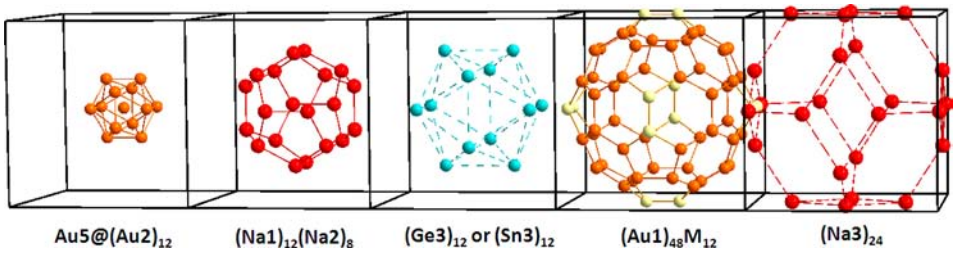

Figure 3. Multiply endohedral shells of clusters in the SB structures of $Na_{26}Au_{40.9}Ge_{14.1}$ (**3**) and $Na_{26}Au_{39.8}Sn_{15.2}$ (**4**). The first four shells define an Au-centered Bergman-type cluster. M means Au/Ge or Au/Sn mixtures. The shells in crystals **1** and **2** have similar geometries, but the decorations for the first and fourth shells are different, and the innermost icosahedral shell in crystal **1** is empty; see the text.

present work certainly yielded more accurate atomic coordinates and refined Au/Ge occupancy at a 12e site. According to powder data, the refined lattice parameters for the present Ge-phase extend over the range of 14.5905(8)−14.5980(8) Å, smaller than 14.62 Å for $Na_{26}Au_{40}Ge_{15}$. The major contrast is the occupation of the Wyckoff 12e site in **4** ($Na_{26}Au_{39.8}Sn_{15.2}$), which is refined well as an Au/Sn mixture (Table 3) (or with admixed vacancies and more Au) (Table S1) rather than as the 1:2 Na/Au mixture reported earlier for $Na_{30}Au_{39}Sn_{12}$.[30] We believe the assignment to Au/Sn mixture is more reasonable because: (1) all M4 sites in **1**−**4** and S**1**−S**3** are consistently occupied by Au and T (T = Ga, Ge, and Sn); (2) such Na/Au mixtures have not been established elsewhere in related systems and are unreasonable in terms of local site potentials; and (3) the calculated powder patterns for **3** and **4** agree very well with the observed powder patterns (Figure S1).

Occupation of Bergman Cluster Centers. As noted above, a significant feature of crystals **2**−**4** is that their innermost Wyckoff 2a (0 0 0) sites are fully occupied by Ga or Au atoms. Therefore, the Pearson symbol for these three phases is *cI*162, rather than the *cI*160 for all other Bergman phases.

Certain interesting correlations (Table 4) are found among the occupation of the Wyckoff 2a site and (1) the size of the innermost icosahedron (r), (2) the size ratio between electropositive and electronegative components (R_+/R_-), and (3) the valence electron counts per atom (e/a values). In general, a larger innermost icosahedron would be necessary to accommodate a guest atom at the center, but the occupation should also depend on the size of the guest atom. For example, although the center-to-vertex values (r) in Bergman structures $Na_{13}Cd_{20}Pd_7$[48] and $Na_{13}Cd_{18.9}Tl_{8.1}$[39] are the largest two values in Table 4, their 2a sites are still empty because the potential guest atoms, Cd, Pd, or Tl, are all too large. Thus, the weighted size ratio (R_+/R_-) between electropositive and electronegative atoms may also be an important factor. As shown in Table 4, the R_+/R_- ratios for all three phases with occupied 2a sites are no less than 1.27, and those with empty icosahedra have smaller R_+/R_- values. The question then arises as to why the 2a site in $Na_{26}Au_{18.1}Ga_{35.9}$ with a large R_+/R_- value (1.34) is not occupied. Besides the small d value, we hypothesize that this is also related to its large e/a value (1.90). As listed in Table 4, the e/a values for the three SB phases are within the range of 1.47−1.56, some measures of the degree of oxidation and the parallel larger Au contents.

It is also of interest to inquire why the 2a sites in $Na_{26}Au_{40.9}Ge_{14.1}$ (**3**) and $Na_{26}Au_{39.8}Sn_{15.2}$ (**4**) are occupied by Au, whereas that in $Na_{26}Au_{36.0}Ga_{19.0}$ (**2**) is occupied by Ga. These are akin to frequently encountered "coloring problems" in solids.[49] Generally, a plot of relative Mulliken populations as a function of the valence electron counts gives useful clues as to the preferred atom types at different crystallographic sites, as is done for Bergman phases $Mg_{2-y}(Zn_xAl_{1-x})_{3+y}$[28] and $Na_{13}(Cd,Tl)_{27}$.[39] In these Au-rich cases (**2**−**4**), a Mulliken population analysis indicates that the 2a sites are valence-electron-poor relative to the other sites and would attract the less electronegative metal, i.e., Ga versus Au as in **2** but Ge or Sn versus Au for **3** and **4**, respectively. This population analysis, however, neglects the effects of all interatomic orbital interactions as well as some of the intrinsic electronic characteristics of Au, i.e., relativistic influences on its valence orbitals that would also affect "coloring". Nevertheless, the e/a values and the center-to-vertex distances (r) may, to some extent, give better clues to the "coloring problem" here. Compared with the Ge- and Sn-containing examples, $Na_{26}Au_{36.0}Ga_{19.0}$ has smaller r and e/a values, both of which might be close to the lower limits for the SB phases. If Ga atoms at the 2a site in $Na_{26}Au_{36.0}Ga_{19.0}$ were to be replaced by larger Au atoms, a higher chemical pressure and lower e/a value (<1.47) could result, the latter meaning the compound might be overoxidized and valence-electron-poor.

Fermi Surface−Brillouin Zone Interactions. Disorder-free models are needed for tight-binding electronic structure calculations. Therefore, the hypothetical models "$Na_{26}Au_{24}Ga_{30}$" and "$Na_{26}Au_{43}Sn_{12}$" with single atom types at all sites were built from CB-type $Na_{26}Au_{18.1}Ga_{35.9}$ (**1**) and the less disordered SB-type $Na_{26}Au_{39.8}Sn_{15.2}$ (**4**) structures by changing (1) the M1, M2, and M4 sites in **1** to Au, Ga, and Ga, respectively, and (2) the M4 site in **4** to Au. Calculations on an alternative model "$Na_{26}Au_{37}Sn_{18}$" with Sn assigned to the M4 site in **2** were also performed, but these led to the same conclusion. Therefore, the following considers the first model "$Na_{26}Au_{43}Sn_{12}$" as representative of the SB phases.

Parts a and b of Figure 4 show the DOS curves for hypothetical "$Na_{26}Au_{24}Ga_{30}$" (CB) and "$Na_{26}Au_{43}Sn_{12}$" (SB), respectively. Because both patterns are continuous around the Fermi level, all CB- and SB-type Na−Au-T phases should be metallic. The peak below −7.0 eV arises mainly from Ga 4s or Sn 5s orbitals, whereas the spiky peaks from −7.0 to 0 eV are dominated by the Au 5d, Na 3s, and 3p and Ga 4p or Sn 5p levels, an outcome that is typical for Au-rich polar intermetallic phases.[50,51] The most significant and relevant features of both DOS curves are the pseudogaps around the Fermi energies, the formation of which can be well explained by Fermi surface−Brillouin zone interactions.[17,50] This effect can be evaluated using the equation $2K_F = \pi/a(h^2 + k^2 + l^2)^{1/2}$, in which K_F is the radius of the Fermi sphere and h, k, and l are the Miller indices of lattice planes with larger diffraction intensities. In this case, the diameter of the Fermi sphere for the hypothetical $Na_{26}Au_{43}Sn_{12}$ is about 1.448 $Å^{-1}$. This value is close to the center-to-face distance (1.479 $Å^{-1}$) of the Brillouin zones

dx.doi.org/10.1021/ic300866q | Inorg. Chem. 2012, 51, 8882−8889

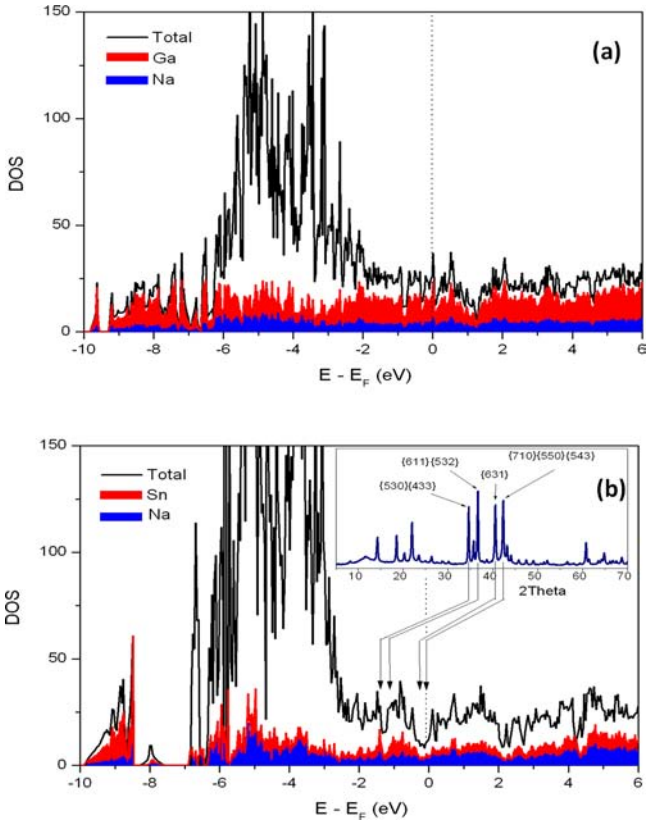

Figure 4. Overlay of the projected DOS of Ga or Sn (red) and Na (blue) in the hypothetical (a) "$Na_{26}Au_{24}Ga_{30}$" (CB) and (b) "$Na_{26}Au_{43}Sn_{12}$" (SB) models. The white area under the total DOS (black) denotes the contributions of Au. The inset in part b shows a partial experimental powder pattern of $Na_{26}Au_{39.83(6)}Sn_{15.17(6)}$ and the correlation between diffraction peaks and pseudogaps in DOS.

constructed from zone planes with $|G|^2 = 50$ ($|G|$, which includes {710}, {550}, and {543} diffractions that correspond to the strong peaks at scattering angles of about 42.3°, as shown in the inset; here $|G|$ is defined as the critical reciprocal lattice vector by Mizutani et al.[50]). In physics, this means the Fermi surface approaches the above-mentioned Brillouin zone polyhedron; thus, electrons on the Fermi surface can also reach the Brillouin zone with a larger surface area. Accordingly, the density of electrons drops at the Fermi energy, i.e., resulting in the formation of a pseudogap. Such Fermi surface–Brillouin zone matching has also been seen in other Bergman-type and even in Tsai-type phases.[17]

The e/a value corresponding to the Fermi level for the CB-type structural model "$Na_{26}Au_{24}Ga_{30}$" is 1.75, a value that is, as a matter of fact, very close to that of the icosahedral quasicrystal $Na_{26}Au_{24}Ga_{30}$ (1.75) discovered in the same system.[31] In comparison, the Fermi level for the "$Na_{26}Au_{43}Sn_{12}$" SB model corresponds to an e/a value of 1.44, smaller than those of crystals **2**–**4** (Table 2). This might be related to the apparent absence of corresponding icosahedral quasicrystals in the Ge and Sn systems. Note also that the Fermi level of the idealized $Na_{26}Au_{43}Sn_{12}$ version of the experimental composition $Na_{26}Au_{39.8}Sn_{15.2}$ is located at the pseudogap at ca. −1.2 eV under rigid band assumptions (Figure 4b).

CONCLUSION

In this work, the CB and SB phases have been synthesized and structurally established in the Na–Au–Ga system. A conventional version, $Na_{26}Au_xGa_{54-x}$, is found in the relatively Au-poor region ($x \approx 18.1$–19.5), whereas the Ga-stuffed versions $Na_{26}Au_yGa_{55-y}$ occur in Au-rich compositions ($y \approx 35.2$–36.0). Although these two types have very similar structures, they do not form a continuous solid solution. Rather, an icosahedral quasicrystal and an orthorhombic derivative of the Bergman phases lie between them.[31] SB phases of $Na_{26}Au_{40.93(5)}Ge_{14.07(5)}$ and $Na_{26}Au_{39.83(6)}Sn_{15.17(6)}$ have also been synthesized and characterized. The latter updates an unlikely refined stoichiometry in the literature with a mixed Au/Na site.[30] However, no CB phases appear to exist in the Ge or Sn systems. The occupation and coloring of the Wyckoff 2a sites in these Bergman phases are found to be related to (1) the sizes of the neighboring icosahedra, (2) the size ratios between electropositive and electronegative components, and (3) the e/a values. The present Bergman phases follow the Hume-Rothery mechanism for electronically and structurally stable intermetallic compounds, with the formation of pseudogaps in the DOS curves arising from interactions between the Fermi surface and Brillouin zone surfaces corresponding to strong diffraction peaks, as usual for other Bergman-type phases.

ASSOCIATED CONTENT

Supporting Information

Crystallographic data for crystals **S1**–**S3** (Tables S1 and S2), experimental and simulated powder patterns of $Na_{26}Au_{40.93(5)}Ge_{14.07(5)}$ and $Na_{26}Au_{39.83(6)}Sn_{15.17(6)}$. (Figure S1), resistivity results for three Bergman phases (Figure S2), and the CIF outputs. This material is available free of charge via the Internet at http://pubs.acs.org.

AUTHOR INFORMATION

Corresponding Author

*E-mail: gmiller@iastate.edu (G.J.M.), jcorbett@iastate.edu (J.D.C.).

Notes

The authors declare no competing financial interest.

ACKNOWLEDGMENTS

We are indebted to Sergey Bud'ko for the resistivity measurements. This research was supported by the U.S. Department of Energy, Office of Basic Energy Sciences, Division of Materials Sciences and Engineering. Ames Laboratory is operated for the U.S. Department of Energy by Iowa State University under Contract DE-AC02-07CH11358.

REFERENCES

(1) Corbett, J. D. *Inorg. Chem.* **2010**, *49*, 13.
(2) Lin, Q.; Corbett, J. D. *Struct. Bonding* **2009**, *133*, 1.
(3) Li, B.; Kim, S.-J.; Miller, G. J.; Corbett, J. D. *Inorg. Chem.* **2009**, *48*, 6573.
(4) Lin, Q.; Corbett, J. D. *Inorg. Chem.* **2011**, *50*, 1808.
(5) Lin, Q.; Corbett, J. D. *Inorg. Chem.* **2007**, *46*, 8722.
(6) Lin, Q.; Corbett, J. D. Unpublished results.
(7) Höckendorf, R. F.; Cao, Y.; Beyer, M. K. *Organometallics* **2010**, *29*, 3001.
(8) Gruene, P.; Rayner, D. M.; Redlich, B.; van der Meer, A. F. G.; Lyon, J. T.; Meijer, G.; Fielicke, A. *Science* **2008**, *321*, 674.
(9) Johnson, G. E.; Wang, C.; Priest, T.; Laskin, J. *Anal. Chem.* **2011**, *83*, 8069.
(10) Bulusu, S.; Li, X.; Wang, L.-S.; Zeng, X. C. *Proc. Natl. Acad. Sci. U.S.A.* **2006**, *103*, 8326.
(11) Li, J.; Li, X.; Zhai, H.-J.; Wang, L.-S. *Science* **2003**, *299*, 864.

(12) Zhang, H.-F.; Stender, M.; Zhang, R.; Wang, C.; Li, J.; Wang, L.-S. *J. Phys. Chem. B* **2004**, *108*, 12259.
(13) Kim, F.; Connor, S.; Song, H.; Kuykendall, T.; Yang, P. *Angew. Chem.* **2004**, *116*, 3759.
(14) Fan, H.; Yang, K.; Boye, D. M.; Sigmon, T.; Malloy, K. J.; Xu, H.; López, G. P.; Brinker, C. J. *Science* **2004**, *304*, 567.
(15) Hume-Rothery, W. *J. Inst. Met.* **1926**, *35*, 295.
(16) Hume-Rothery, W.; Raynor, G. V. *The Structure of Metals and Alloys*, 4th ed.; Institute of Metals: London, 1962.
(17) Mizutani, U. In *The Science of Complex Alloy Phases*; Massalski, T. B., Turchi, P. E. A., Eds.; The Minerals, Metals & Materials Society: Warrendale, PA, 2005; p 1.
(18) Li, B.; Kim, S.-J.; Miller, G. J.; Corbett, J. D. *Inorg. Chem.* **2009**, *48*, 11108.
(19) Smetana, V.; Corbett, J. D.; Miller, G. J. *Inorg. Chem.* **2011**, *51*, 1695.
(20) Lin, Q.; Corbett, J. D. *Inorg. Chem.* **2008**, *47*, 7651.
(21) Lin, Q.; Corbett, J. D. *Inorg. Chem.* **2008**, *47*, 3462.
(22) Lin, Q.; Corbett, J. D. *J. Am. Chem. Soc.* **2007**, *129*, 6789.
(23) Lin, Q.; Corbett, J. D. *Inorg. Chem.* **2010**, *49*, 4570.
(24) Lin, Q.; Corbett, J. D. *Inorg. Chem.* **2010**, *49*, 10436.
(25) Pauling, L. *The Nature of the Chemical Bond*, 3rd ed.; Cornell University Press: IthacaNY, 1960; p 403.
(26) Smetana, V.; Miller, G. J.; Corbett, J. D. *Inorg. Chem.* **2012**, *51*, 7711.
(27) Bergman, G.; Waugh, J. L. T.; Pauling, L. *Acta Crystallogr.* **1957**, *10*, 254.
(28) Lee, C.-S.; Miller, G. J. *J. Am. Chem. Soc.* **2000**, *122*, 4937.
(29) Sun, W.; Lincoln, F. J.; Sugiyama, K.; Hiraga, K. *Mater. Sci. Eng., A* **2000**, *294–296*, 327.
(30) Doering, W.; Schuster, H. U. *Z. Naturforsch.* **1979**, *34b*, 1757.
(31) Smetana, V.; Lin, Q.; Pratt, D. K.; Kreyssig, A.; Ramazanoglu, M.; Corbett, J. D.; Goldman, A. I.; Miller, G. J., submitted for publication.
(32) *SHELXTL*, 6.10 ed.; Bruker Analytical X-ray Systems, Inc.: Madison, WI, 2000.
(33) Gelato, L. M.; Parthé, E. *J. Appl. Crystallogr.* **1987**, *20*, 139.
(34) Tank, R.; Jepsen, O.; Burkhardt, A.; Andersen, O. K. *TB–LMTO–ASA Program*, version 4.7; Max-Planck-Institut für Festkörperforschung: Stuttgart, Germany, 1994.
(35) Shriver, H. L. *The LMTO Method*; Springer-Verlag: Berlin, Germany, 1984.
(36) Jepsen, O.; Snob, M. Linearized Band Structure Methods. *Electronic Band-Structure and its Applications*; Springer Lecture Notes; Springer-Verlag: Berlin, Germany, 1987.
(37) Andersen, O. K.; Jepsen, O. *Phys. Rev. Lett.* **1984**, *53*, 2571.
(38) Lambrecht, W. R. L.; Andersen, O. K. *Phys. Rev. B* **1986**, *34*, 2439.
(39) Li, B.; Corbett, J. D. *Inorg. Chem.* **2004**, *43*, 3582.
(40) Lee, C.-S.; Miller, G. J. *Inorg. Chem.* **2000**, *40*, 338.
(41) Tillard-Charbonnel, M.; Belin, C. *J. Solid State Chem.* **1991**, *90*, 270.
(42) Frank-Cordier, U.; Cordier, G.; Schaefer, H. *Z. Naturforsch.* **1982**, *B37*, 119.
(43) Frank-Cordier, U.; Cordier, G.; Schaefer, H. *Z. Naturforsch.* **1982**, *B37*, 126.
(44) Ling, R. G.; Belin, C. *Acta Crystallogr., Sect. B* **1982**, *38*, 1101.
(45) Zachwieja, U. *Z. Anorg. Allg. Chem.* **1996**, *622*, 1173.
(46) Lin, Q.; Corbett, J. D. *Proc. Natl. Acad. Sci. U.S.A.* **2006**, *103*, 13589.
(47) Takakura, H.; Pay Gómez, C.; Yamamoto, Y.; De Boissieu, M.; Tsai, A. P. *Nat. Mater.* **2007**, *6*, 58.
(48) Todorov, E.; Sevov, S. C. *Inorg. Chem.* **1997**, *36*, 4298.
(49) Miller, G. J. *Eur. J. Inorg. Chem.* **1998**, *1998*, 523.
(50) Lin, Q.; Corbett, J. D. *Inorg. Chem.* **2011**, *50*, 11091.
(51) Mizutani, U.; Takeuchi, T.; Fournee, V.; Sato, H.; Banno, E.; Onogi, T. *Scr. Metall.* **2001**, *44*, 1181.
(52) Audier, M.; Pannetier, J.; Leblanc, M.; Janot, C.; Lang, J.-M.; Dubost, B. *Phys. B* **1988**, *153*, 136.
(53) Elding-Pontén, M.; Lidin, S. *J. Solid State Chem.* **1995**, *115*, 270.